EMIT: A Discrete Reaction–Diffusion–Potential Model Exhibiting Robust Bubble Formation and Convergent Macroscopic Observables

Neal Hawkins

February 2, 2026

Abstract

EMIT is a 2D discrete-time, continuous-field dynamical system that couples (i) Gray–Scott reaction–diffusion dynamics on fields (U, V), (ii) a threshold conversion of excitation into an accumulated mass-like field M, and (iii) a Poisson potential Φ sourced by M that induces transport of V down potential gradients. We present EMIT as a reproducible computational framework for studying emergent "bubble-like" domains and for stress-testing macroscopic observables under numerical variation, rather than as a calibrated physical theory. Using 13 structured test suites (40 runs total), we evaluate Δt sweeps, grid refinement and Δx rescaling, CFL-style scaling ($\Delta t \propto \Delta x^2$), seed repeatability, and an exploratory effective local PDE-fit diagnostic.

We identify a compact falsifiable observable within the model family: the dominant oscillation frequency f_{peak} of the operational bubble radius $R(t)$, computed from a windowed FFT and summarized by a tail-median statistic. In the plateau protocol (Test 8; $N = 256$, $\Delta t = 1.0$), f_{peak} converges to the same tail-median value (0.001397) across five independent seeds (tail IQR 0.000579). In continuum mode at fixed resolution (Test 11; $N = 256$, $\Delta x = 1/256$), the final physical-radius proxy $R\,\Delta x$ varies by 0.23% across $\Delta t \in \{0.25, 0.5, 1.0\}$. Under refinement with $\Delta t \propto \Delta x^2$ (Test 6B), $R\,\Delta x$ exhibits a convergent trend between $N = 256$ and $N = 512$ (relative difference 0.48%). All reported quantities are in simulation units. All configurations, logs, and analysis scripts are packaged for reproduction.

1 Introduction

Discrete, rule-based systems can produce rich macroscopic behavior that is often difficult to anticipate from the update rule alone. Reaction–diffusion systems, in particular, are known to generate spontaneous pattern formation from homogeneous states [1], and the Gray–Scott cubic-autocatalysis family provides a widely studied minimal model exhibiting rich spatiotemporal structure [2, 3]. EMIT is a computational model designed to explore whether a small set of interacting operations—propagation, conversion, potential-driven transport, and decay—can generate stable "bubble-like" domains and repeatable macroscopic observables.

The contribution of this work is primarily methodological and reproducibility-driven:

- A fully specified update operator (Section 2) with explicit state variables and parameters.
- A logging protocol with per-frame metrics and event traces.
- A battery of robustness tests (Section 3) covering Δt sweeps, resolution sweeps, and seed sweeps.
- A packaged analysis script that regenerates all plots and tables from raw logs.

2 Model definition

2.1 State variables

EMIT evolves a periodic 2D grid with fields:

- $U(x, y)$: Gray–Scott substrate (bounded $[0, 1]$).
- $V(x, y)$: excitation/energy-like field (bounded $[0, v_{\max}]$).
- $M(x, y)$: frozen mass-like accumulator (bounded $[0, m_{\max}]$).
- $T(x, y)$: time dilation map for the next step (bounded $[T_{\min}, 1]$).
- Optional wave driver $(W, \dot{W})$ used as a controlled perturbation channel.

A Poisson potential $\Phi(x, y)$ is computed each step from M and used to advect V.

2.2 Update operator

Figure 1 summarizes the operator. Each step applies:

1. **Diffusion on** V: $V \leftarrow V + D_E \nabla^2 V \, \Delta t$ (with optional continuum rescaling by Δx).
2. **Gray–Scott reaction–diffusion** on (U, V) [2,3]:
$$\partial_t U = D_u \nabla^2 U - UV^2 + F(1 - U), \quad \partial_t V = D_v \nabla^2 V + UV^2 - (F + k)V.$$
3. **Threshold freeze**: where $V > \theta$, transfer $\Delta M = \alpha V \Delta t$ from V into M.
4. **Secondary emission**: a kernel-filtered pulse from ΔM adds back to V scaled by β.
5. **Potential + advection**: solve $\nabla^2 \Phi = \kappa(M - \langle M \rangle)$ on a periodic grid (implemented with FFT-based spectral inversion), then update V via a conservative transport term proportional to $\nabla \cdot (V \nabla \Phi)$ [4,5].
6. **Cleanup/decay**: apply damping and floors to V; apply exponential decay and optional diffusion to M.
7. **Time dilation**: compute $T = 1/(1 + \lambda M)$ and clip to $[T_{\min}, 1]$.

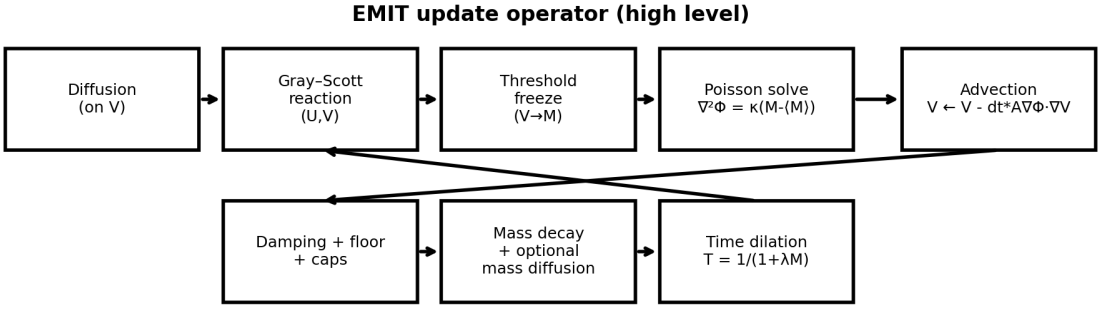

Figure 1: High-level EMIT update operator used for all reported experiments.

parameter	value
A_adv	0.18
D_E	0.02
D_u	0.16
D_v	0.08
F	0.035
alpha	0.04
beta	0.1
bubble_thresh	0.15
damping	0.001
display_gamma	1
dt	1
floor	5e-05
k	0.065
kappa	0.6
m_cap	5
mass_decay	0.0002
mass_release	0.0008
min_area	10
min_component_area	10
theta	0.32
time_dilation	0.7
time_floor	0.25
v_cap	5

Table 1: Baseline parameter values (example run). All sweeps in this paper vary only the indicated parameters (e.g., Δt, grid size, Δx) while keeping the remainder fixed unless stated.

2.3 Parameters

Table 1 lists baseline parameter values. In the reported test suites, we vary Δt, grid size N, and (where applicable) Δx under a "continuum mode" that applies Δx scaling to differential operators.

3 Methods

3.1 Test suite structure and logging

We report 13 test suites (including a CFL-style variant labeled 6B). Each run logs:

- `frames.csv`: per-frame time series (radius R, component counts, totals, frequency estimates, and diagnostics).
- `events.csv`: user actions and discrete events.
- `config.json`: full configuration, including all parameter values.
- Optional `snapshots/` images at fixed frame intervals.

3.2 Primary observable

The primary falsifiable observable reported here is the dominant oscillation frequency of the bubble radius, f_{peak}, computed from a windowed FFT of $R(t)$ (as logged in `frames.csv`). For each run

we summarize a tail statistic: median f_{peak} over the final 30% of non-missing frequency frames.

3.3 Integrity checks

We validate that `frame` and `t` are monotonic, required columns exist, and that any missing values occur only in intermittently computed diagnostics (e.g., FFT-derived features). All 40 runs passed these checks.

4 Results

4.1 Qualitative evolution

Figure 2 shows representative snapshots at early, mid, and late times for a scaling run, illustrating the emergence and stabilization of structured domains.

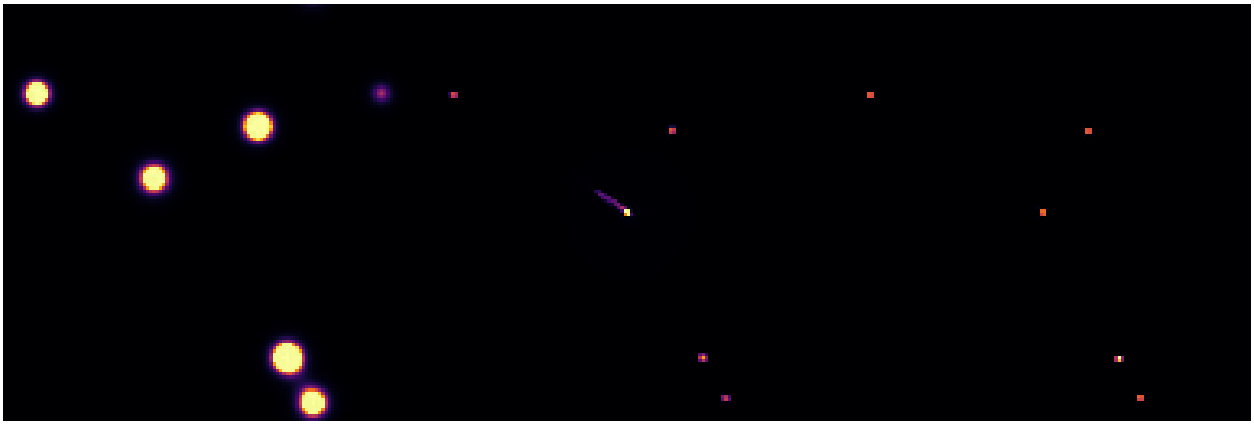

Figure 2: Representative evolution snapshots (three time points) from a scaling run (Test 5; N=128, dt=0.5).

4.2 Example time series

Figure 3 reports $R(t)$, component counts, the dominant frequency, and a rolling variance stability diagnostic for a representative run.

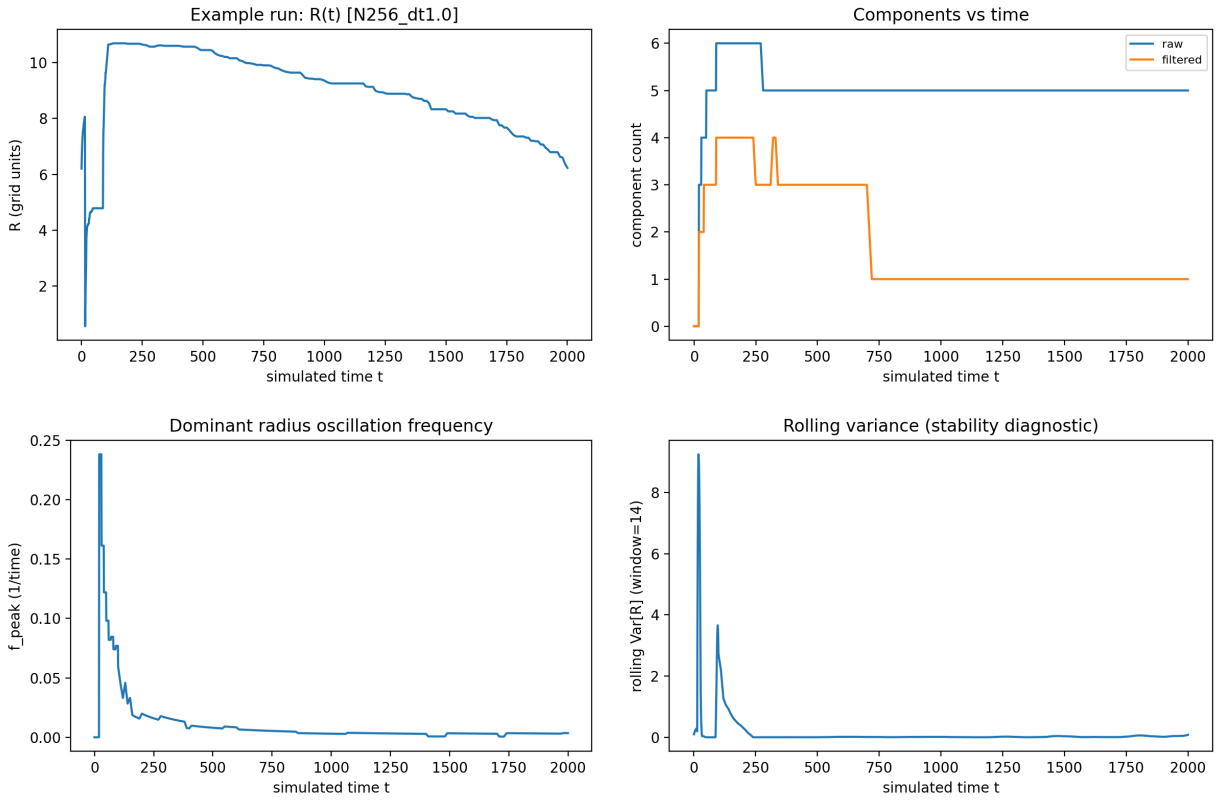

Figure 3: Example run diagnostics: bubble radius, component counts, dominant frequency estimate, and rolling variance of radius.

4.3 Seed repeatability of the plateau prediction

In the plateau test (Test 8), five different random seeds yield an identical stabilized dominant frequency, with f_{peak} tail-median equal to 0.001397 for all seeds (standard deviation 0.000000). This provides a compact, falsifiable prediction within the model family: under the baseline configuration and plateau protocol, the radius oscillation frequency converges to a reproducible value.

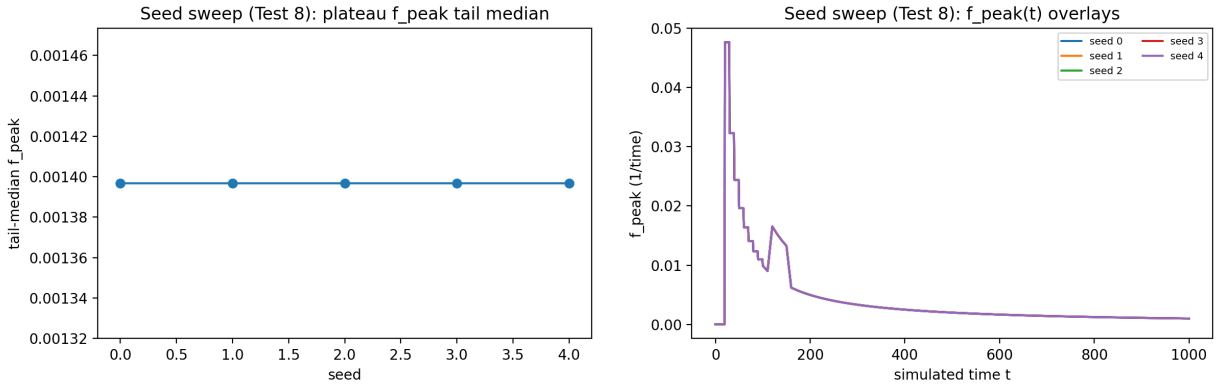

Figure 4: Seed sweep (Test 8): (left) tail-median f_{peak} per seed; (right) $f_{\text{peak}}(t)$ overlays.

4.4 Time-step robustness in continuum mode

At fixed resolution ($N = 256$, $\Delta x = 1/256$), a Δt sweep in continuum mode (Test 11; same protocol as Test 7) shows that the final physical-radius proxy $R\,\Delta x$ remains stable across $\Delta t \in \{0.25, 0.5, 1.0\}$, with mean 0.444698 and standard deviation 0.001038 (relative variation $\approx 0.23\%$). The corresponding $R\,\Delta x(t)$ overlays are shown in Figure 5.

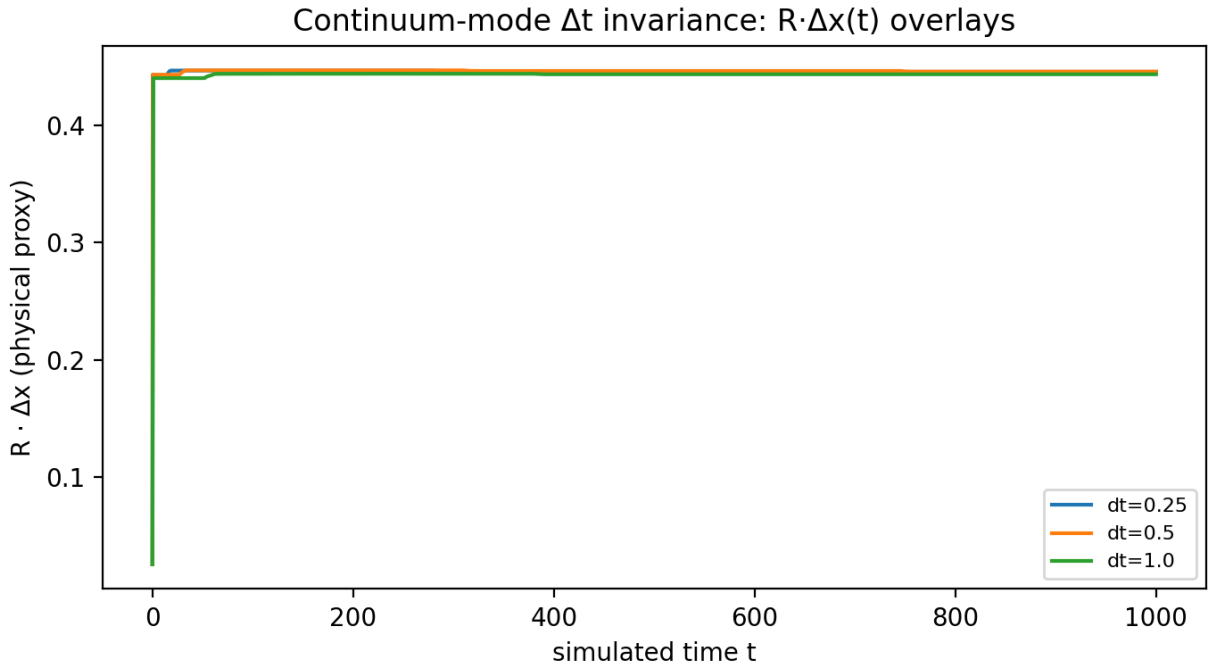

Figure 5: Continuum-mode Δt invariance (Test 11; same protocol as Test 7): $R\,\Delta x(t)$ overlays at fixed $N = 256$ and fixed Δx.

4.5 Refinement trend under CFL-style scaling

Under refinement with $\Delta t \propto \Delta x^2$ (Test 12; replicated independently in Test 6B), the proxy $R\,\Delta x$ shows a convergent trend between $N = 256$ and $N = 512$:

$$R\,\Delta x(N = 256) \approx 0.443235, \quad R\,\Delta x(N = 512) \approx 0.441102,$$

with relative difference $\approx 0.48\%$, while the coarser $N = 128$ case deviates (≈ 0.545865). Figure 6 summarizes this scaling.

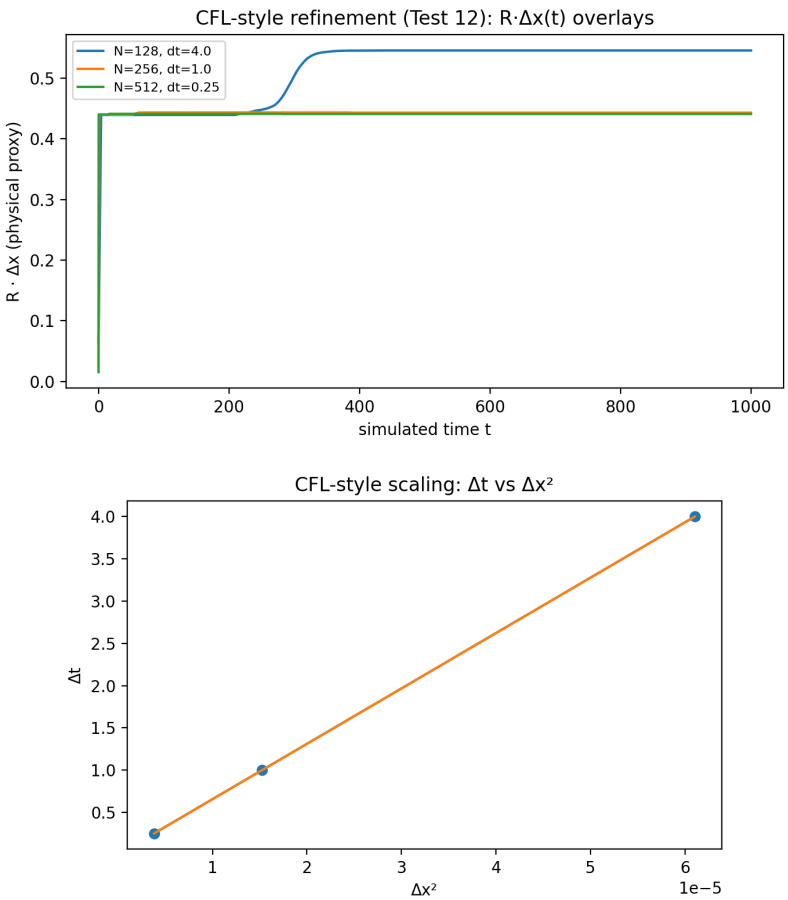

Figure 6: CFL-style scaling (Test 12): (top) $R\,\Delta x(t)$ overlays for $N \in \{128, 256, 512\}$ with matched $\Delta t \propto \Delta x^2$; (bottom) the Δt vs Δx^2 relationship.

4.6 Effective local PDE fit diagnostic

Test 9 logs an effective local linear fit diagnostic (`fit_r2`) used as a proxy for whether macroscopic radius dynamics are locally well-approximated by a simple low-order model. Figure 7 shows the evolution of this fit quality over time.

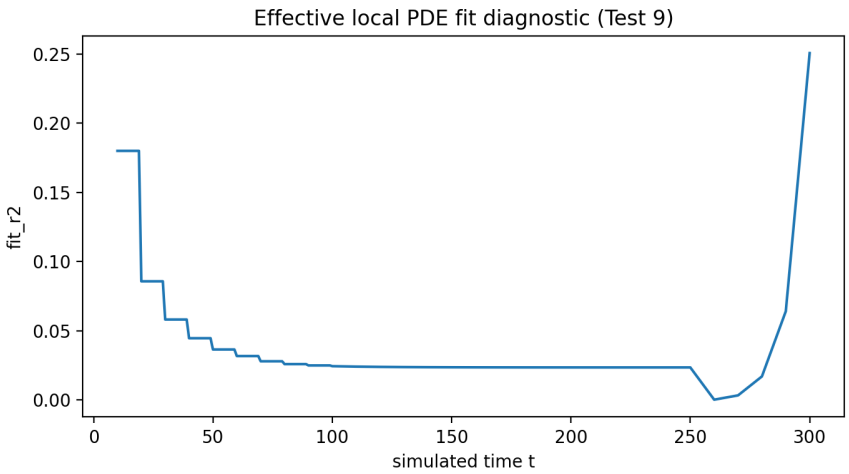

Figure 7: Effective PDE-fit quality diagnostic (Test 9): R^2 of a local linear fit over time.

5 Discussion

The experiments show that the EMIT update operator—reaction–diffusion pattern formation coupled to threshold conversion and potential-driven transport—can yield stable macroscopic domains together with repeatable summary statistics. The strongest single reproducibility result in the current suite is the seed-invariant plateau frequency in Test 8: under a fixed protocol, the tail-median f_{peak} is identical across five independent seeds. Because f_{peak} is computed directly from the logged radius time series $R(t)$ and summarized using an explicit tail statistic, this constitutes a clear model-internal prediction that can be reproduced (or falsified) from the provided run folders.

The continuum-mode experiments further suggest that, once Δx scaling is applied to differential operators, selected macroscopic quantities become only weakly dependent on Δt over a practical range. At fixed resolution ($N = 256$), the proxy $R\,\Delta x$ varies at the sub-percent level across a Δt sweep. The CFL-style refinement experiments indicate that $R\,\Delta x$ approaches a consistent value between $N = 256$ and $N = 512$ when Δt is reduced proportionally to Δx^2, while the coarser $N = 128$ case deviates. Taken together, these results are consistent with (but do not prove) the existence of a numerically stable macroscopic regime for this model class.

Interpretation should remain strictly model-internal. The fields U, V, M and derived quantities such as R and f_{peak} are operational definitions within EMIT, and no mapping to physical units or observational datasets is claimed here. The contribution of this paper is therefore best viewed as (i) an explicit operator definition, (ii) a reproducible logging and analysis pipeline, and (iii) a set of robustness and refinement tests that quantify which observables are stable under numerical variation and which are sensitive to numerical or algorithmic choices.

6 Limitations and future work

- **Model status:** This work evaluates robustness of EMIT's internal observables; it does not calibrate parameters to physical units, constants, or datasets.
- **Operational observables:** The "bubble" mask and radius R depend on thresholding and connectivity definitions; future work should include threshold-sensitivity sweeps and alternative morphology summaries (e.g., perimeter, eccentricity, multipole moments).

- **Dimensionality and boundaries:** All experiments are 2D with periodic boundary conditions; extension to 3D and explicit multi-bubble interaction tests are needed before making claims about broader applicability.
- **Conservation diagnostics:** While the update includes clipping, floors, and decay terms, explicit conservation or balance laws are not enforced. Adding conserved variants and reporting budget terms would strengthen mechanistic interpretation.
- **Exploratory diagnostics:** The effective PDE-fit statistic (`fit_r2`) is exploratory and should be treated as a heuristic; future work should benchmark it against known synthetic dynamics and report sensitivity to windowing choices.
- **Broader parameter sensitivity:** The current test battery focuses on Δt, Δx, N, and seeds. Systematic sweeps over core couplings (e.g., κ, A_{adv}, α, β) are required to map regime structure and failure modes.

Data and code availability

All run folders (including `config.json`, `frames.csv`, and `events.csv`), representative snapshots, and the analysis script used to regenerate figures and tables are included in the accompanying submission package. The reproduction command is provided at the end of the paper.

A Response to external review and feedback (template)

This appendix is provided as a structured response framework; it can be expanded as additional external feedback arrives. Any externally sourced critique referenced here should be interpreted as *informal feedback* rather than an official review or endorsement by any institution.

- **Claim discipline:** This paper does not claim a complete theory of everything. It reports a computational model and reproducible tests.
- **Reproducibility:** All runs and scripts are packaged. One-command regeneration is provided in `code/analysis.py`.
- **Numerical robustness:** We include Δt sweeps, Δx refinement trends, and CFL-style scaling tests.
- **Falsifiable observable:** The plateau frequency statistic in Test 8 provides a concise prediction within the model family.

B Reproducibility instructions

From the submission root:

```
python -m venv .venv
. .venv/bin/activate   # Windows: .venv\Scripts\activate
pip install -r code/requirements.txt

python code/analysis.py --data data --out _regen
```

Expected outputs:

- `_regen/tables/run_summary.csv`
- `_regen/figures/*.png`

References

[1] A. M. Turing, *The Chemical Basis of Morphogenesis*, Philosophical Transactions of the Royal Society of London. Series B, Biological Sciences **237**(641), 37–72 (1952). doi:10.1098/rstb.1952.0012.

[2] P. Gray and S. K. Scott, *Autocatalytic reactions in the isothermal, continuous stirred tank reactor: Oscillations and instabilities in the system $A + 2B \rightarrow 3B$; $B \rightarrow C$*, Chemical Engineering Science **39**(6), 1087–1097 (1984). doi:10.1016/0009-2509(84)87017-7.

[3] J. E. Pearson, *Complex Patterns in a Simple System*, Science **261**(5118), 189–192 (1993). doi:10.1126/science.261.5118.189.

[4] R. W. Hockney and J. W. Eastwood, *Computer Simulation Using Particles*, 2nd ed. (Adam Hilger, Bristol, 1988).

[5] W. H. Press, S. A. Teukolsky, W. T. Vetterling, and B. P. Flannery, *Numerical Recipes in C: The Art of Scientific Computing*, 2nd ed. (Cambridge University Press, Cambridge, 1992).